Covenant Journal of Engineering Technology (CJET) Vol.1 No. 2, Dec. 2017

An Open Access Journal Available Online

Crevice Corrosion Behavior of Nickel-Based Alloy 718 in both Aerated and De-Aerated Chloride Environment

F. Bakare[1, 2], J. Ugorji[1], Y. Alsubhi[1], S. Okunzuwa[2] & A. Orobor[3]

[1]School of Materials, University of Manchester,
Manchester, M13 9PL, United Kingdom
[2]Department of Physics, University of Benin,
Benin City, Edo, Nigeria
[3]Department of Mechanical Engineering, University of Benin,
Benin City, Nigeria
folarin.bakare@uniben.edu (Corresponding Author),
jarminugorji@gmail.com,
subhiys@aramco.com,
okunzuwas@yahoo.com,
awheme.oghenerobor@uniben.edu

***Abstract*:** In this study, anodic potentiodynamic polarization techniques were used to study the crevice corrosion behaviour of Nickel alloy 718 (with and without a crevice former) in both aerated and de-aerated solution of 3.5wt% sodium chloride solution. Surface observation of the specimens after each experiment was done with the optical microscope. The results showed that crevice corrosion were initiated at potentials as low as 520mVSCE, while the surface observation on the specimen with a crevice former revealed that the crevice corrosion attack was restricted under the crevice gap and at the border areas of the crevice former but did not occur at the surfaces outside the shielded areas. Conversely, the specimen without a crevice former showed evidence of waterline corrosion. These results can be attributed to the development of differential oxygen concentration in the specimen depending on the exposure of the parts to dissolved oxygen. This study has developed a more comprehensive understanding of the crevice corrosion

initiation mechanism and behaviour of Nickel-based Alloy 718 under applied crevice torques, chloride environment and exact potentials, thereby leading to better prevention and control of localized corrosion in this alloy.

Keywords: Nickel-based alloy 718; localized corrosion; Crevice corrosion; polarization curve; crevice former;

1.0 Introduction

Nickel based alloy 718 has recently gained extensive use for constructing the downhole assembly of the drilling rig employed in the oil and gas industries due to its excellent combination of mechanical properties, corrosion resistance and non-magnetic properties [1-5]. In more details, the candidacy of alloy 718 for the downhole drilling activities has been attributed to the order strengthening of the γ'' - phase, precipitation hardening of γ' - particles in the γ -matrix and the balanced additions of Chromium (Cr) and Molybdenum (Mo) alloying elements, especially at temperatures as high as 650℃ [6]. The alloying elements of Cr and Mo has been found to form dense oxide/hydroxide films when exposed to aqueous electrolytes or moist air [7].However, the mechanical and electrochemical interaction between surfaces in relative motion and in the presence of corrosive environment (Tribocorrosion) typical of those encountered in drilling processes can remove the passive film, as a result, exposing the surface of the alloy substrate, thereby giving rise to anodic dissolution of the alloy. For instance, the presence of significant concentrations of chlorides, hydrogen sulphide (H_2S), carbon dioxide (CO_2) coupled with the high operating temperatures especially in the deeper wells of oil and gas exploration has greatly hampered the performance of Nickel-based alloy 718, and has generated attention from researchers to mitigate or eliminate the failure of this alloy by pitting corrosion, crevice corrosion, environmental assisted cracking including hydrogen embrittlement and stress corrosion cracking [8-11]. Kehler et al [12] investigated the crevice corrosion stabilization of Nickel-based alloys (625 and 22) and concluded that it is been influenced by temperature and electrolyte composition but not by the pH of the bulk solution. Additionally, she successfully assessed the crevice corrosion resistance of these alloys by relating the voltage dependent crevice corrosion rate to the open-circuit potentials. McCoy and his colleagues [13] reviewed the materials selection of Nickel-based alloys on the basis of an excellent blend of mechanical and corrosion properties for simulated (sweet and sour) oilfield requirements. Hayes et al [14] performed a post-localized breakdown analysis by introducing Cr and Mo in specified amounts to Nickel-based alloy and noticed that the passivity of the alloy was maintained and stabilized after a localized breakdown event. Mishra et al [15] determined the crevice re-passivation potential and temperature for Alloy 22 (UNS06022) using Tsujikawa-Hisamatsu electrochemical technique (THE). Amin et al [16] attempted and succeeded to reduce the tribocorrosion issues in Nickel-based alloy 718 by adding about 2.5-3.5% amount of Rhenium (Re) to the matrix. It was pointed out that 6% additions only increased the rate of uniform and pitting corrosion processes. Mishra et al

[17] studied the role of alloying elements in a number of commercially available Nickel-based alloys under several aggressive environments by evaluating the weight loss, electrochemical changes and surface characterization techniques. Due to the scarce literature of the corrosion behaviour between air and anaerobic conditions in the presence of chloride ions. The study of the corrosion kinetics in the above mentioned environment could prove useful due to the difference in oxygen concentration as the depth of downhole drilling increases. Consequently, there is need to study the crevice corrosion behaviour of this alloy in different microstructural conditions under a synergistic simulated corrosive environment of chloride ions in both aerated and de-aerated form in order to separate the effect of oxygen from the rate of rotation as a result of applied torque and to analyze the corrosion kinetics by surface characterization and anodic potentiodynamic polarization techniques.

2.0 Materials and Methods

Commercial Nickel-based alloy 718 (UNS N07718) samples with dimensions of 19.73x19.73x2.44mm in the mill-annealed condition were used in this experiment. The chemical composition of the alloy is shown in Table 1 below.

Table 1: Nominal composition of Nickel-based Alloy 718 [18].

Element	**Al**	**C**	**Co**	**Cr**	**Cu**	**Fe**	**Mo**	**Ti**	**Nb**	**Ni**
mass %	0.52	0.021	0.11	19.06	0.02	18.15	3.04	0.93	5.08	53.0

For the electrochemical experiments, a stainless steel wire was spot welded to the specimens to establish an electrical connection with the specimen. This was then covered with a plastic tube, held to the spot welded area with an adhesive and the uncovered surface area of the spot weld was coated with a protective epoxy resin to prevent electrical conductivity and formation of fine crevices. The crevice assembly consists of a steel metal fastener (Nut and bolt with washers) to secure the crevice assembly and a crevice former with dimension (outer diameter – 16.02mm, inner diameter – 4.06mm and thickness – 6.40mm). Potentiodynamic polarization in 3.5% NaCl solution was carried out in both aerated and de-aerated condition. The specimens were used as the working electrode while a platinum electrode and saturated calomel electrode (SCE) were used as counter and reference electrode respectively. The three electrodes were appropriately connected to the Potentiostat (Ivium Compactstat) whose output data was digitally recorded on the computer software (Iviumsoft). Two tests were carried out for each set of experiments at room temperature with aeration; one test specimen without crevice assembly and the other with crevice assembly to actually ascertain the effect of crevice former (crevice torque applied) and the potential at which crevice corrosion initiates on the alloy in this particular test environment.

A total of three sets of experiments were carried out with different crevice torques applied (0.5Nm, 1.0Nm and 1.5Nm respectively). Before the potentiodynamic scans were conducted, the test specimens were allowed to stabilize in the test solution at open-circuit for 120s. The potentiodynamic polarization scans were conducted from 300mVSCE below the open-circuit Potential, Eocp in the anodic direction with scan rate of 1mV/s and limiting current density of 100 μA/cm2. The sweeps was set to end in the forward direction without reversing when the potential reaches 1500mVSCE.

The crevice corrosion potential Ecrev was identified as the point at which crevice corrosion initiates (the point at which there is an increase in current), to enable effective analysis and understanding of the crevice corrosion behaviour of alloy 718 in chloride environment. The same set of experiments described above were carried out but in de-aerated environment where a constant flow of nitrogen gas was bubbled into the solution for about 30minutes to reduce the dissolved oxygen concentration in the solution before the start of the potentiodynamic polarization scan and the flow rate was reduced and maintained until the end of the scan. The same crevice torque of 1.5Nm was used for the four sets of experiments while the scan started 300mVSCE below the open-circuit potential and final point of the scans were set at 300mVSCE, 1200mVSCE and 1500mVSCE respectively. This was to actually ascertain the effect of the various potentials on the surface of the specimen and the potential at which at which crevice corrosion starts to initiate. After each experiment, the specimens were dismantled, allowed to dry for 10munites and visualized using the OLYMPUS optical microscope with $\times 5$ magnification.

3.0 Results

3.1 Potentiodynamic polarization in aerated 3.5wt% sodium chloride (NaCl) with and without crevice former

The potentiodynamic polarization scan was done at various set potentials to produce a reproducible results to develop the standard electrochemical parameters to image the crevice corrosion behaviour of Nickel alloy 718 (UNS N07718).

Fig. 1 shows the potentiodynamic polarization scan results obtained where the final scan points were set at 300mVSCE, 600mVSCE, 900mVSCE, 1200mVSCE and 1500mVSCE respectively. However for a clearer analysis of the plot, Fig. 2 which shows the potentiodynamic polarization scan at final scan point of 1200mVSCE and applied crevice torque of 1.5Nm was concentrated upon. It can be observed that the specimen exhibits passive behaviour at the early stages of the potentiodynamic polarization scan until at about 520mVSCE and limiting current density of $10^{-5.8}$A/cm^2. Although corrosion was observed in both specimens with the crevice former and those without the crevice former, corrosion on the specimen without the crevice former seems to be waterline corrosion. As the potential increased in the anodic direction, the passive region remained constant until about the potential of 520mVSCE when there was a sharp increase in the current density from $10^{-5.8}$A/cm^2 to $10^{-4.3}$A/cm^2.

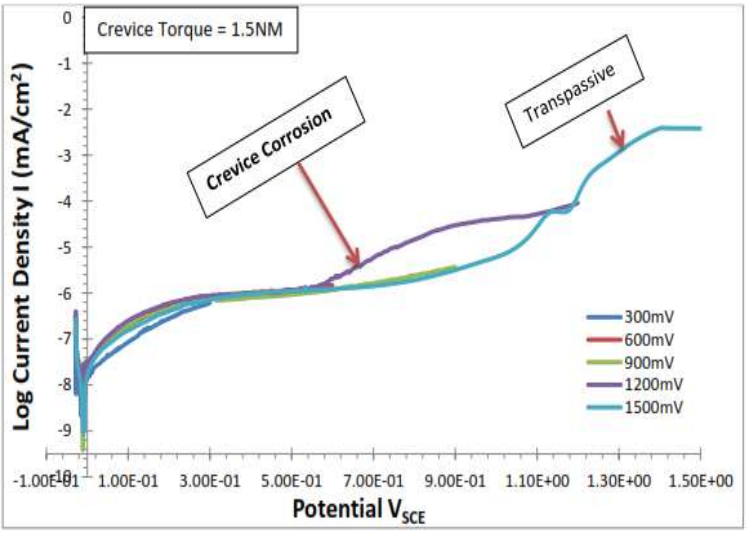

Fig. 1: Potentiodynamic polarization scan in aerated solution of 3.5wt% sodium chloride with crevice former at final scan point of 300mVSCE, 600mVSCE, 900mVSCE, 1200mVSCE and 1500mVSCE and crevice torque of 1.5Nm

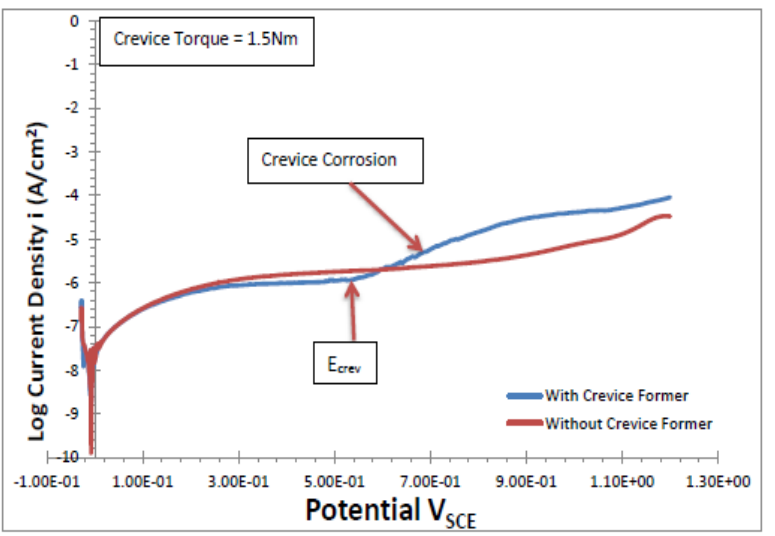

Fig. 2: Potentiodynamic polarization scan in aerated solution of 3.5wt% sodium chloride with and without crevice former at final scan point of 1200mVSCE and applied crevice torque of 1.5Nm showing crevice corrosion attack on the specimen.

Fig. 3 shows the optical micrographs of the various specimens (with and without a crevice former) of nickel alloy 718 after potentiodynamic

polarization in 3.5wt% aerated sodium chloride solution at (a) 1500mVSCE (b) 1200mVSCE, (c) 900mVSCE (d) 600mVSCE (e) 300mVSCE. Although there were no traces of crevice corrosion between 300-900mVSCE, but some form of artefacts were present probably due to either surface grinding or surface etching resulting from poor sample preparation. Crevice starts to initiate at the border area of the crevice former but did not develop at either the inner surface of the shielded area by the crevice former or the surface outside the crevices at scan points of 1200mVSCE. Corrosion attack was also observed on specimens without the crevice former at the final point scan of 1500mVSCE mainly at the water-line area

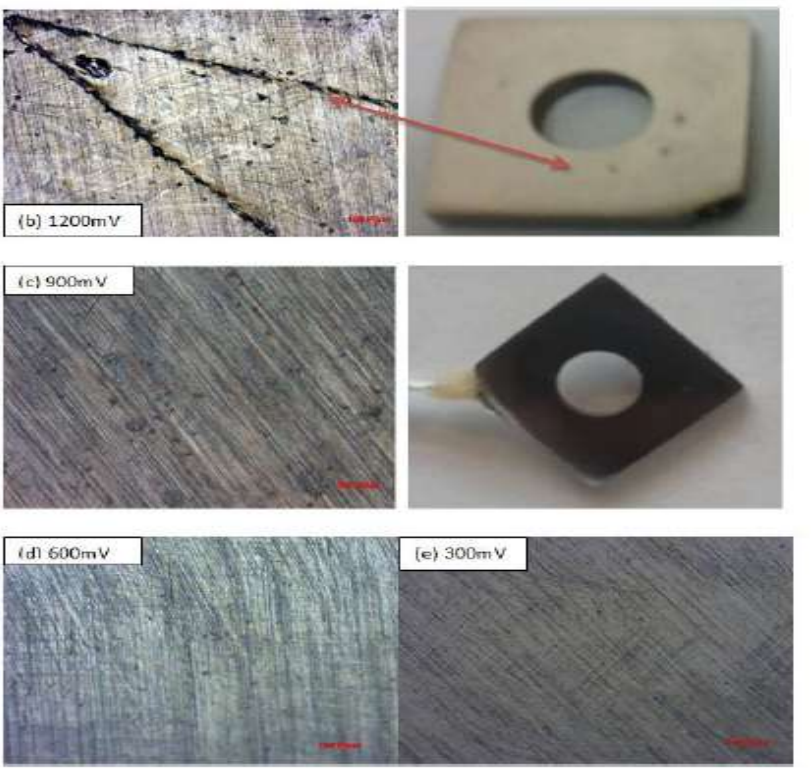

Fig. 3: Optical surface examination of nickel alloy 718 specimen with crevice former after potentiodynamic polarization in 3.5wt% aerated sodium chloride solution at (a) 1500mVSCE (b) 1200mV SCE, (c) 900mVSCE (d) 600mVSCE (e) 300mVSCE.

Fig. 4 shows the optical micrographs of nickel alloy 718 without a crevice former after potentiodynamic polarization in 3.5wt% aerated sodium chloride solution at (a) 1500mVSCE (b) 1200mV SCE (c) 900mVSCE, (d) 600mVSCE, and (e) 300mVSCE respectively. The waterline corrosion was visible only at the potential of 1500mVSCE and not for 1200mVSCE, 900mVSCE, 600mVSCE, 300mVSCE respectively

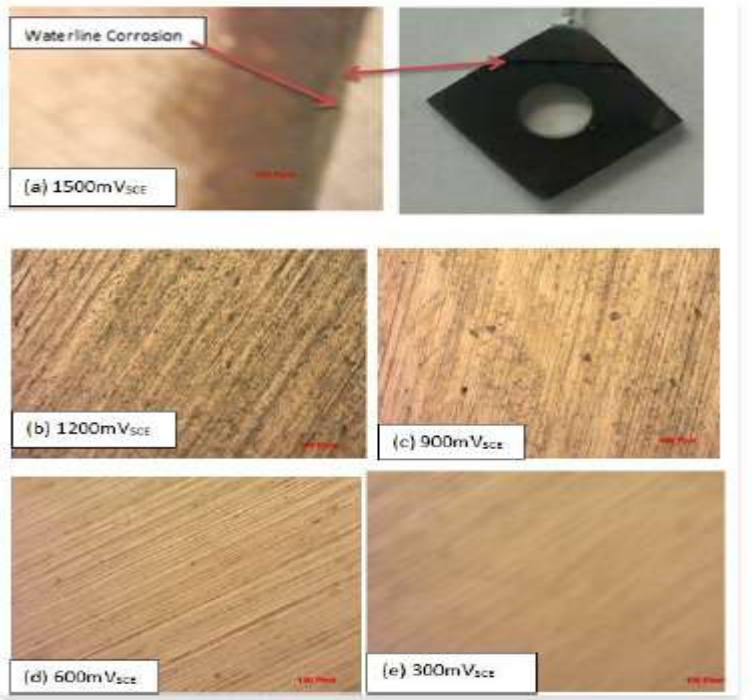

Fig. 4: Optical micrographs of nickel alloy 718 specimen without crevice former after potentiodynamic polarization in 3.5wt% aerated sodium chloride solution at (a) 1500mVSCE (b) 1200mV SCE (c) 900mVSCE (d) 600mVSCE and (e) 300mVSCE.

3.2 Potentiodynamic polarization in de-aerated 3.5wt% sodium chloride (NaCl) with and without crevice former and at different scan points

The same sets of experiments discussed earlier were conducted but in the de-aerated solution with and without crevice former and at final point scans of 300mVSCE, 1200mVSCE, and 1500mVSCE.

The potentiodynamic polarizations scan in de-aerated solution of 3.5wt% sodium chloride at different scan points (Fig. 5 and 6), with and without a crevice former (Fig. 7) is presented below. In the presence of a crevice former, crevice corrosion was observed at final scan point of 1500mVSCE. It will be observed from the graph that the crevice corrosion initiated (Ecrev) was at the potential of about 530mVSCE, which is approximately the same point in the aerated environment. Whereas in the absence of crevice former, the increase in current observed on the graph as pictured in Fig. 6 is at the potential of about 870mVSCE. No crevice corrosion was observed at final scan points of 1200mVSCE and 300mVSCE as shown in Fig. 6 below. In Fig. 7, a rapid increase in current which coincides with crevice corrosion initiation above the passive current density were observed at about a potential of 530mVSCE at final scan points of 1500mVSCE as found in the aerated environment, but with a difference in potential of about 10mVSCE.on comparison with Fig. 2 above.

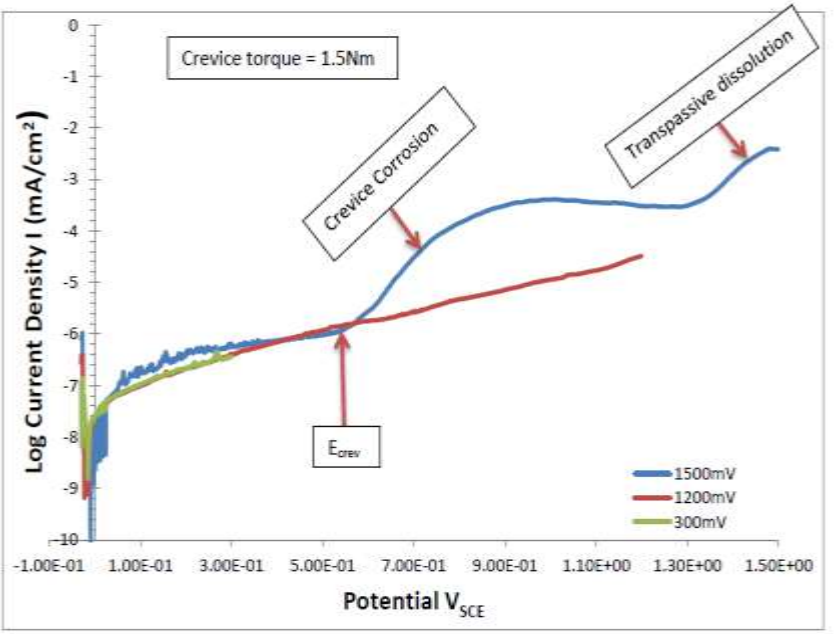

Fig. 5: Potentiodynamic polarization scan in deaerated solution of 3.5wt% sodium chloride with crevice former at final scan point of 1500mVSCE, 1200mVSCE and 300mVSCE

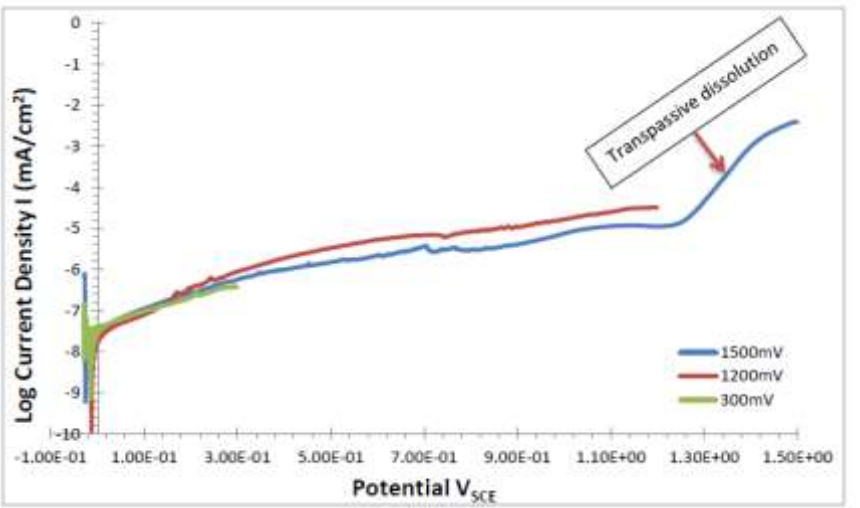

Fig. 6: Potentiodynamic polarization scan in deaerated solution of 3.5wt% sodium chloride without crevice former at final scan point of 1500mVSCE, 1200mVSCE and 300mVSCE

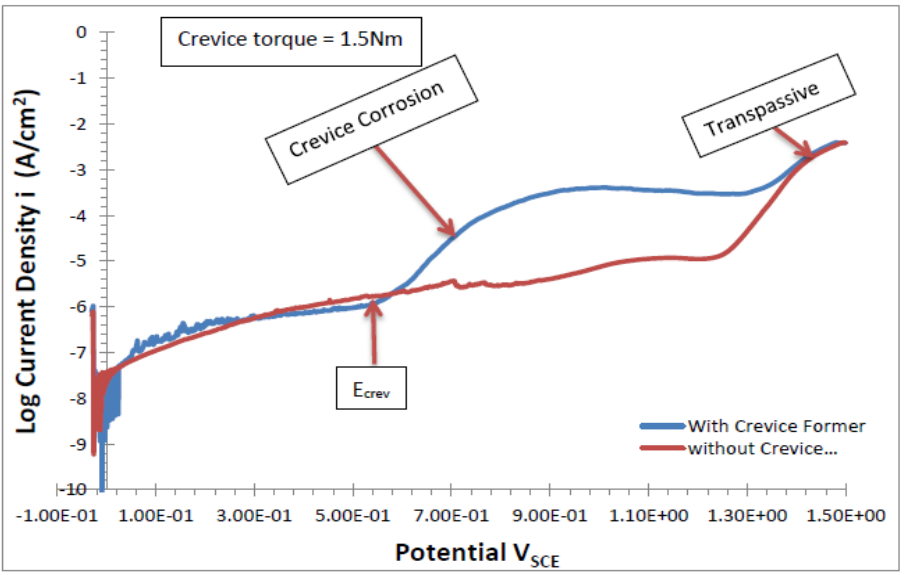

Fig. 7: Potentiodynamic polarization scan in deaerated solution of 3.5wt% sodium chloride with and without crevice former at final scan point of 1500mVSCE

The surface examination of the test specimens were carried out as shown in Fig. 8 and 9. When a crevice former is present as shown in Fig. 8, crevice corrosion was observed at final scan point of 1500mVSCE which correlates with the result shown on the potentiodynamic polarization plot in Fig. 5 and 6. Additionally, crevice corrosion was seemingly initiating at final scan point of 1200mVSCE but this was not evident in the polarization plot. The black de-colouration could probably be some form of artefact due to either surface grinding or surface etching resulting from the crevice corrosion process. There was no evidence of crevice corrosion at final scan point of 300mVSCE. Fig. 9 shows the surface examination (Optical microscopy) of nickel alloy 718 specimen without crevice former after potentiodynamic polarization in 3.5wt% de-aerated sodium chloride solution at 1500mVSCE (b) 1200mV SCE and (c) 300mVSCE. Some little forms of transpassive metal dissolution were observed at the final scan point of 1500mVSCE and there was no evidence of corrosion at final scan point of 1200mVSCE and 300mVSCE respectively.

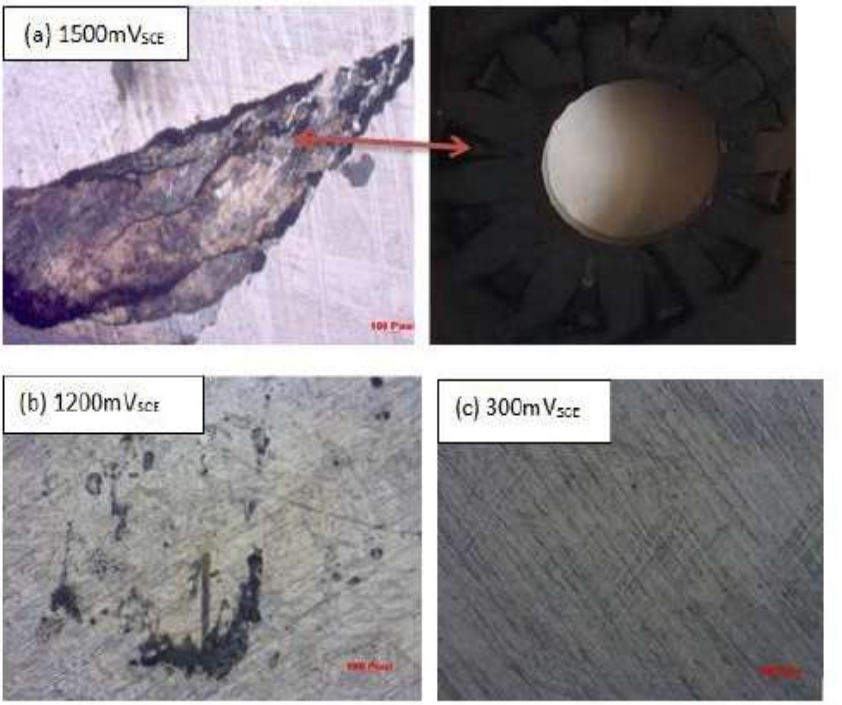

Fig. 8: Optical micrograph of nickel alloy 718 specimen with crevice former after potentiodynamic polarization in 3.5wt% de-aerated sodium chloride solution at1500mVSCE (b) 1200mV SCE and (c) 300mVSCE.

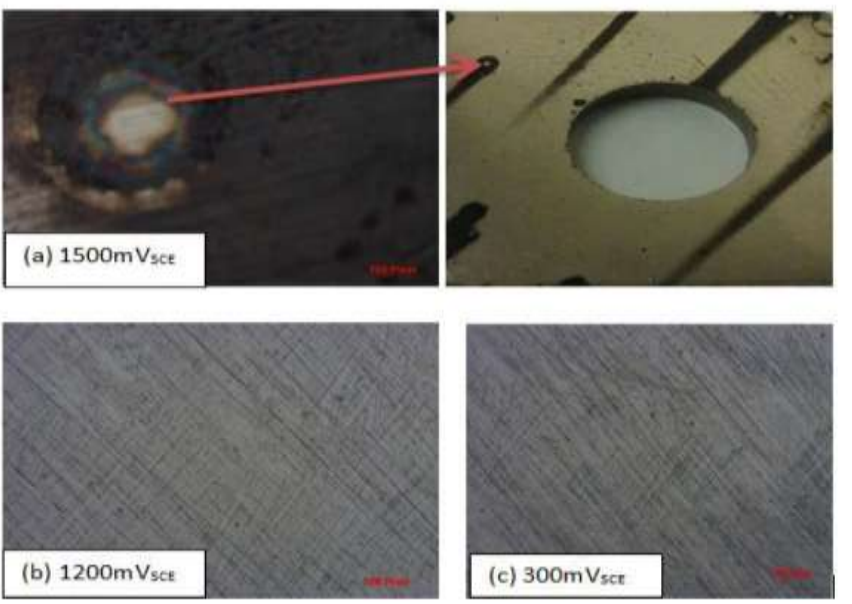

Fig. 9: Optical micrographs of nickel alloy 718 specimen without crevice former after potentiodynamic polarization in 3.5wt% de-aerated sodium chloride solution at 1500mVSCE (b) 1200mVSCE and (c) 300mVSCE

4.0 Discussion

The sharp increase in the current density as observed in Fig. 1 is an evidence of crevice corrosion in the aerated solution of 3.5wt% sodium chloride with crevice former where the final scan point was set 1200mVSCE and applied crevice torque of 1.5Nm. The waterline corrosion in the sample without the crevice former could be attributed to the development of a differential oxygen concentration cell as suggested by Palanna [20] and subsequent deposition of electrons (rust) at the waterline area. The part of the specimen immersed lower in the solution (anode) is exposed only to less dissolved oxygen than the part higher in the solution (cathode), which is in direct contact with atmospheric oxygen. This causes corrosion to take place at the anode while the cathode is free from corrosion.

The corrosion initiation at scan points of 1200mVSCE in the presence of a crevice former conforms to the fact that crevice corrosion initiates preferentially from the crevice mouth (border area of crevice former) and moves towards the centre of the crevice former according to [21] at this particular potential. This also validates that crevice corrosion does not occur outside crevices as opined by Rashidi et al [22]. In the absence of crevice former, the visible waterline corrosion only at the potential of 1500mVSCE and not for 1200mVSCE, 900mVSCE, 600mVSCE, 300mVSCE respectively is due to differential aeration as discussed earlier.

The current increase observed in Fig. 5 could be attributed to the transpassive metal dissolution of the alloy. This was not observed at final scan point of 300mVSCE and 1200mVSCE because the potentials were not high enough to cause transpassivity.

5.0 Conclusion

The crevice corrosion behaviour of Nickel based alloy (Alloy 718 UNS N07718) in 3.5wt% sodium chloride has been studied using the potentiodynamic polarization electrochemical method. The microscopic observation of the surface of the alloy after each of the experiments was conducted. The following conclusions can be drawn:

1. Crevice corrosion was observed to occur on the specimen with a crevice former in aerated solution of 3.5wt% of sodium chloride from the polarization curve.
2. The surface observation with the optical microscope revealed that crevice corrosion attack was restricted under the crevice gap and at the border areas of the crevice former but did not occur at the surfaces outside the shielded areas**,** which shows the effect of the crevice former on crevice corrosion initiation of nickel-based alloy 718 (UNS N07718).
3. Waterline corrosion occurred on the specimens partially immersed into the solution of 3.5wt% of sodium chloride without a crevice former. This can be attributed to the development of a differential oxygen concentration.
4. This study can be used to validate the fact that crevice corrosion is a stochastic process as pointed out by Schweitzer et al [9] and can occur at potentials as low as 520mVSCE. Moreover, It will guide the development of standard electrochemical parameters to image the crevice corrosion behaviour of Nickel alloy 718 (UNS N07718).

References

[1] Onyewuenyi, O., 1989. Alloy 718--Alloy Optimization for Applications in Oil and Gas Production. *Superalloy 718: Metallurgy and Applications*, pp.345-362.

[2] Slama, C. and Abdellaoui, M., 2000. Structural characterization of the aged Inconel 718. *Journal of alloys and compounds*, *306*(1), pp.277-284.

[3] Bhavsar, R. B., Collins, A., & Silverman, S. (2001). Use of alloy 718 and 725 in oil and gas industry. *Minerals, Metals and Materials Society/AIME, Superalloys 718, 625, 706 and Various Derivatives(USA),*, 47-55.

[4] Yin, Z.F., Zhao, W.Z., Lai, W.Y. and Zhao, X.H., 2009. Electrochemical behaviour of Ni-base alloys exposed under oil/gas field environments. *Corrosion Science*, *51*(8), pp.1702-1706.

[5] Chen, T., John, H., Xu, J., Lu, Q., Hawk, J. and Liu, X., 2014. Influence of surface modifications on pitting corrosion behavior of nickel-base alloy 718. Part 2: Effect of aging treatment. *Corrosion Science*, *78*, pp.151-161.

[6] Hertweck, B., Steigerwald, T.G., Alt, N.S. and Schluecker, E., 2014. Different corrosion behaviour of autoclaves made of nickel base alloy 718 in ammonobasic and ammonoacidic environments. *The Journal of Supercritical Fluids*, *95*, pp.158-166.

[7] Zhang, X. and Shoesmith, D.W., 2013. Influence of temperature on passive film properties on Ni–Cr–Mo Alloy C-2000. *Corrosion Science*, *76*, pp.424-431.

[8] Behrens, R. and Agarwal, D.C., 2005, January. Laboratory Testing Of Age-Hardenable Alloys Environments 925 And 718 In Sour Gas: Proc. of Corrosion 2005 Conf., Houston, Texas: NACE Int., 2005, Paper No. 05103. .

[9] Aberle, D. and Agarwal, D.C., 2008, January. High performance corrosion resistant stainless steels and nickel alloys for oil & gas applications: Proc. of Corrosion 2008 Conf.,

Houston, Texas: NACE Int., 2008, Paper No. 08085

[10] Macdonald, K.A. and Bjune, J.V., 2007. Failure analysis of drillstrings. *Engineering Failure Analysis*, *14*(8), pp.1641-1666.

[11] Antunes, R.A. and de Oliveira, M.C.L., 2012. Corrosion fatigue of biomedical metallic alloys: mechanisms and mitigation. *Acta biomaterialia*, *8*(3), pp.937-962.

[12] Kehler, B.A., Ilevbare, G.O. and Scully, J.R., (2001). Crevice corrosion stabilization and re-passivation behavior of Alloy 625 and Alloy 22. *Corrosion*, *57*(12), pp.1042-1065.

[13] McCoy, S. A., Hereford, U. K., Puckett, B. C., Hibner, E. L., & Huntington, W. V. (2002). High performance age-hardenable nickel alloys solve problems in sour oil and gas service. *Balance*, *14*(5), 16-23.

[14] Hayes, J.R., Gray, J.J., Szmodis, A.W. and Orme, C.A., 2006. Influence of chromium and molybdenum on the corrosion of nickel-based alloys. *Corrosion*, *62*(6), pp.491-500.

[15] Mishra, A.K. and Frankel, G.S., 2008. Crevice corrosion repassivation of alloy 22 in

aggressive environments. *Corrosion*, *64*(11), pp.836-844.

[16] Amin, M.A., El-Bagoury, N., Saracoglu, M. and Ramadan, M., 2014. Electrochemical and Corrosion Behavior of cast Re-containing Inconel 718 Alloys in Sulphuric Acid Solutions and the Effect of Cl. *Int. J. Electrochem. Sci*, *9*, pp.5352-5374.

[17] Mishra, A., Shoesmith, D. and Manning, P., 2016. Materials Selection for Use in Concentrated Hydrochloric Acid. *Corrosion*, *73*(1), pp.68-76.

[18] Thomas, A., El-Wahabi, M., Cabrera, J. M., & Prado, J. M. (2006). High temperature deformation of Inconel 718. *Journal of materials processing technology*, *177*(1), 469-472.

[19] Ren, X., Sridharan, K., & Allen, T. R. (2007). Corrosion behavior of alloys 625 and 718 in supercritical water. *Corrosion*, *63*(7), 603-612.

[20] Palanna, O. G. (2009). *Engineering chemistry*. Tata McGraw-Hill Education.

[21] He, X., & Dunn, D. S. (2007). Crevice corrosion penetration rates of alloy 22 in chloride-containing waters. *Corrosion*, *63*(2), 145-158.

[22] Rashidi, N., Alavi-Soltani, S. R., & Asmatulu, R. (2007). Crevice corrosion theory, mechanisms and prevention methods.

[23] Schweitzer, P. A. (1996). *Corrosion Engineering Handbook, -3 Volume Set*. CRC Press.